

Article

Evaluation of Structural Stability, Mechanical Properties, and Corrosion Resistance of Magnesia Partially Stabilized Zirconia (Mg-PSZ)

Dedek Yusuf ¹, Eneng Maryani ², Deby Fajar Mardhian ^{3,4}  and Atiek Rostika Noviyanti ^{1,*} 

¹ Department of Chemistry, Universitas Padjadjaran, Jl. Raya Bandung Sumedang Km 21, Jatinangor, Sumedang 45361, Jawa Barat, Indonesia; dedek17002@mail.unpad.ac.id

² Center for Ceramics, Ministry of Industry of Indonesia, Jl. Ahmad Yani 392, Bandung 40272, Jawa Barat, Indonesia; enengmaryani@kemenperin.go.id

³ Department of Dental Materials Science and Technology, Faculty of Dentistry, Universitas Padjadjaran, Jl. Raya Bandung Sumedang Km 21, Jatinangor, Sumedang 45361, Jawa Barat, Indonesia; d.fajar.mardhian@unpad.ac.id

⁴ Oral Biomaterials Research Center, Faculty of Dentistry, Universitas Padjadjaran, Jl. Sekeloa Selatan I No. 1, Bandung 40132, Jawa Barat, Indonesia

* Correspondence: atiek.noviyanti@unpad.ac.id

Abstract: Nano Zirconia (ZrO_2) has been used in dental implants due to having excellent mechanical properties and biocompatibility that match the requirements for the purpose. Zirconia undergoes phase transformation during heating: monoclinic (room temperature to 1170 °C), tetragonal (1170 °C to 2370 °C), and cubic (>2370 °C). Most useful mechanical properties can be obtained when zirconia is in a multiphase form or in partially stabilized zirconia (PSZ), which is achieved by adding small amounts of a metal oxide dopant, such as MgO (magnesia). This study aimed to synthesize nano Mg-PSZ from a local resource found in West Kalimantan, Indonesia, and examine its structural stability, biochemical stability, and mechanical properties. Nano Mg-PSZ was prepared from a zircon local to Indonesia, from West Kalimantan Province, $MgSO_4 \cdot 7H_2O$, and polyethylene glycol (PEG)-6000 was used as a template. The obtained $t-ZrO_2$ after calcination at 800 °C was shown to be stable at room temperature. The highest percentage of the $t-ZrO_2$ phase was obtained at $Zr_{0.95}Mg_{0.05}O_2$ with a variation of 99.5%. The hardness of Mg-PSZ increased from 554 MPa for ZrO_2 without MgO doping to 5266 MPa for ZrO_2 with a doping of 10% MgO. An in vitro biodegradation test showed that the greater the concentration of MgO in doping the ZrO_2 , the greater the degradation resistance of Mg-PSZ in simulated body fluid (SBF) solution.

Keywords: nano-Mg-PSZ; zirconia; dental implants



Citation: Yusuf, D.; Maryani, E.; Mardhian, D.F.; Noviyanti, A.R. Evaluation of Structural Stability, Mechanical Properties, and Corrosion Resistance of Magnesia Partially Stabilized Zirconia (Mg-PSZ). *Molecules* **2023**, *28*, 6054. <https://doi.org/10.3390/molecules28166054>

Academic Editor: Ruijin Yu

Received: 17 July 2023

Revised: 8 August 2023

Accepted: 9 August 2023

Published: 14 August 2023



Copyright: © 2023 by the authors. Licensee MDPI, Basel, Switzerland. This article is an open access article distributed under the terms and conditions of the Creative Commons Attribution (CC BY) license (<https://creativecommons.org/licenses/by/4.0/>).

1. Introduction

Zirconia (zirconium dioxide, ZrO_2), also referred to as “ceramic steel”, has optimal properties for the use of dental implants due to its superior toughness, strength and resistance, excellent wear properties, and biocompatibility [1–3]. Amongst the commonly used materials in dentistry, zirconia has the advantage of being compatible for osteoblasts to adhere and proliferate [4]. It is known that the material in dental implant applications must be biocompatible, have antibacterial activity and low toxicity, be stable and resistant to corrosion, and have high performance for survival in the complex mouth environment [5–8].

Zirconia is known to have three types of crystal: monoclinic ($m-ZrO_2$), tetragonal ($t-ZrO_2$), and cubic ($c-ZrO_2$). The ZrO_2 phase is unstable and can undergo structural transformations such as $t-ZrO_2$ to $m-ZrO_2$ [9]. Metastable tetragonal zirconia is able to transform stress-assisted into the monoclinic state at an ambient temperature if an external load is applied [10]. At room temperature, ZrO_2 is in the form of a monoclinic phase, whereas to obtain the tetragonal and cubic phases requires a sintering temperature [11].

However, in several syntheses using lower calcination temperatures, tetragonal and cubic phases of ZrO_2 were obtained [1,12].

Zirconia with tetragonal and cubic structures are generally obtained by adding a stabilizer to the ZrO_2 lattice structure [13]. Stabilized zirconia generally consist of two or more mixtures of different ZrO_2 phases and is usually obtained by adding metal oxide dopants such as yttria (Y_2O_3) or magnesia (MgO) to the ZrO_2 lattice [3,14]. Stabilized zirconia is a promising material due to its great physical and chemical properties, and thermal stability [15]. Yttria stabilized zirconia (Y-PSZ) is a zirconia-based dental implant material that is often used. However, Y_2O_3 as a ZrO_2 stabilizer is relatively expensive. Therefore, other metal oxides are needed as zirconia stabilizers. When compared with Y-PSZ, magnesium-stabilized zirconia (Mg-PSZ) shows promising characteristics in several aspects, including good mechanical and thermal properties, good stability in low temperature degradation (LTD), and the same coefficient of thermal expansion as YSZ [16–18]. Therefore, Mg-PSZ composite has the potential as a dental implant application material at a relatively low price [1].

As we know, there are three crystallographic phases of zirconia, but it is known that the tetragonal phase ($t-ZrO_2$) has better mechanical properties and corrosion resistance than the monoclinic and cubic phases [19,20]. In previous studies, $t-ZrO_2$ was successfully stabilized by adding MgO as a stabilizer and using a low calcination temperature of 800 °C to produce Mg-PSZ. The use of MgO as much as 1, 5, and 10% *w/w* succeeded in stabilizing ZrO_2 in tetragonal and cubic forms at room temperature [1]. In addition to stabilizing the tetragonal zirconia phase, the addition of 25% MgO concentration increased the hardness (Vickers) of ZrO_2 from 554 to 6350 MPa and fracture strength from 5.2 to 25 MPa. The increase in the mechanical properties of the sample was caused by the formation of the $t-ZrO_2$ phase due to the presence of MgO as a stabilizer, which prevents the reverse allotropic transformation of zirconia so as to maintain the $t-ZrO_2$ phase at room temperature [21]. The lower porosity of the $t-ZrO_2$ phase compared with the other phases causes the corrosion resistance of $t-ZrO_2$ to be better than the $m-ZrO_2$ and $c-ZrO_2$ phases [19]. The addition of MgO as a stabilizer increased the hardness of ZrO_2 and gave 50% better wear performance than ZrO_2 without the addition of MgO [22].

The template method utilizing polyethylene glycol (PEG) is expected to affect the characteristics of ZrO_2 , including changing the morphology of the Mg-PSZ particles. PEG long chains play a role in helping the distribution of metal ions homogeneously and not clumping or settling in the solution so that magnesia-stabilized zirconia is obtained in nano size [14,23]. PEG attaches to the $ZrO(OH)_2$ molecule through hydrogen bonds. The hydroxyl group of the ZrO_2 precursor is covered by a PEG molecule so that aggregation occurring between particles is reduced. During calcination, organic substances are burned as gas, leaving the particles in the nanostructures [14]. This phenomenon reduces the aggregation of synthesized Mg-PSZ particles, so that, in previous studies, Mg-PSZ was obtained with a nano-sized particle diameter of 9–44 nm [1].

In this paper, the mechanical properties and corrosion resistance of Mg-PSZ will be tested. Based on ISO 13356:2015 Third Edition, dental implant materials have a hardness level of 11.8 GPa and the number of monoclinic phases is limited to 20% mass fraction. The Mg-PSZ precursors used in this study were ZrO_2 derived from local zirconium silicate-based zirconium hydroxide, an MgO stabilizer from a $MgSO_4 \cdot 7H_2O$ precursor, and polyethylene glycol (PEG) as a template. This research is expected to determine the mechanical properties, corrosion resistance, and antibacterial activity of Mg-PSZ before continuing to direct application as dental implants.

2. Results and Discussion

2.1. Crystal-Phase Structure Mg-PSZ

The chemical composition of the $ZrO(OH)_2$ precursor was first evaluated using the ARL QUANT'X EDXRF Analyzer. Semi-quantitative XRF analysis was carried out to determine the purity of the local zircon and its contents [24]. The results of the XRF analysis

shown in Table 1. It showed that $\text{ZrO}(\text{OH})_2$ contained 79.24 wt% ZrO_2 and 11.06 wt% MgO , which would be taken into account in the next process to determine each molar ratio of each specimen. The ZrO_2 was then prepared from $\text{ZrO}(\text{OH})_2$ after washing with water [1].

Table 1. XRF analysis of $\text{ZrO}(\text{OH})_2$ precursors.

Compound	Weight %
ZrO_2	79.2400
MgO	11.0600
SiO_2	7.7600
HfO_2	0.5780
MoO_3	0.5700
Y_2O_3	0.4230
Cs_2O	0.1660
Fe_2O_3	0.0344
CdO	0.0339
CuO	0.0331
K_2O	0.0290
Ag_2O	0.0205
SrO	0.0201

The mechanism of Mg-PSZ synthesis is the same as in previous studies [1]. The absorption bands in the range of 400–4000 cm^{-1} show several vibrational modes of strain and chemical bonding in the $\text{Zr}_{0.90}\text{Mg}_{0.10}\text{O}_2$ sample and PEG-6000 functional group. Mg-O bonds appear at 617.72 cm^{-1} , associated with the stretching vibrations of Mg-O bonds, while the Zr-O bond appears at 439.8 cm^{-1} . As shown by the FT-IR analysis in Figure 1, it was observed that the precursor ZrO_2 reacted with PEG degraded at pH 3 during synthesis, producing Zr-(ethylene glycolate) $_n$ and releasing water molecules on heating. PEG hydrogel degradation can occur through hydrolysis due to the presence of strong acids in the form of H_2SO_4 , where the ester bond in the PEG polymer chain will be broken and produce ethylene glycolate as a monomer [25]. The degradation of PEG-6000 at pH 3 was supported by the very low intensity and weak peaks of the CH_2 - strain vibration at 2921.17 cm^{-1} and 2870.738 cm^{-1} compared with the normal PEG which shows a high intensity and strong peaks of the CH_2 strain vibration around 2890 cm^{-1} [1,2,14,26,27]. Then, heating, which is carried out at a temperature of 120 °C, can cause PEG-6000 to be degraded through a thermal degradation mechanism in which the heat and steam provided will facilitate the PEG's decomposition [28]. Thermal degradation refers to the breakdown of the molecules of a substance due to overheating, generally related to polymers, in this case PEG-6000 [29].

After drying at 120 °C (Figure 2), the XRD analysis results showed a strong peak at 2θ of 20°, indicating the presence of ZrSiO_4 , a commonly found Zr mineral [30]. This specimen was likely derived from the $\text{ZrO}(\text{OH})_2$, which contained SiO_2 and led to the formation of ZrSiO_4 . Zirconium silicate is produced from the mineral zircon, which is mined from sand deposits containing several percent zircon and separated by gravity, where it is known as powdered zirconium silicate or as zircon flour [31]. As explained previously, our ZrO_2 precursor comes from local Indonesian zircon and the purification process carried out in previous studies [1] has not 100% separated the zircon and silicate. Therefore, the presence of the silicates is very likely to occur. Interestingly, we observed the presence of $t\text{-ZrO}_2$, as shown in Figure 2, at the 2θ 30° region. This specimen was confirmed by JCPDS PDF2 no. 791770 and confirmed the previous research that found that the addition of MgO caused the formation of $t\text{-ZrO}_2$. However, our study differs from previous studies on Mg-PSZ composites. We conducted this study using a doping mechanism to obtain $t\text{-ZrO}_2$ and observed changes in the mechanical properties and stability of MgPSZ. The addition of certain stabilizers to the zirconia alloy can help maintain the tetragonal structure at room temperature [32]. The stabilizer used in this research is MgO, which can control the transformation of the stress-inducing phase from $t\text{-ZrO}_2$ to other phases. Based on

previous studies regarding the MgPSZ composite, t -ZrO₂ was obtained at 800 °C, but with the doping mechanism in this study at 120 °C, t -ZrO₂ could be formed. However, further testing is required to determine the stability of the t -ZrO₂.

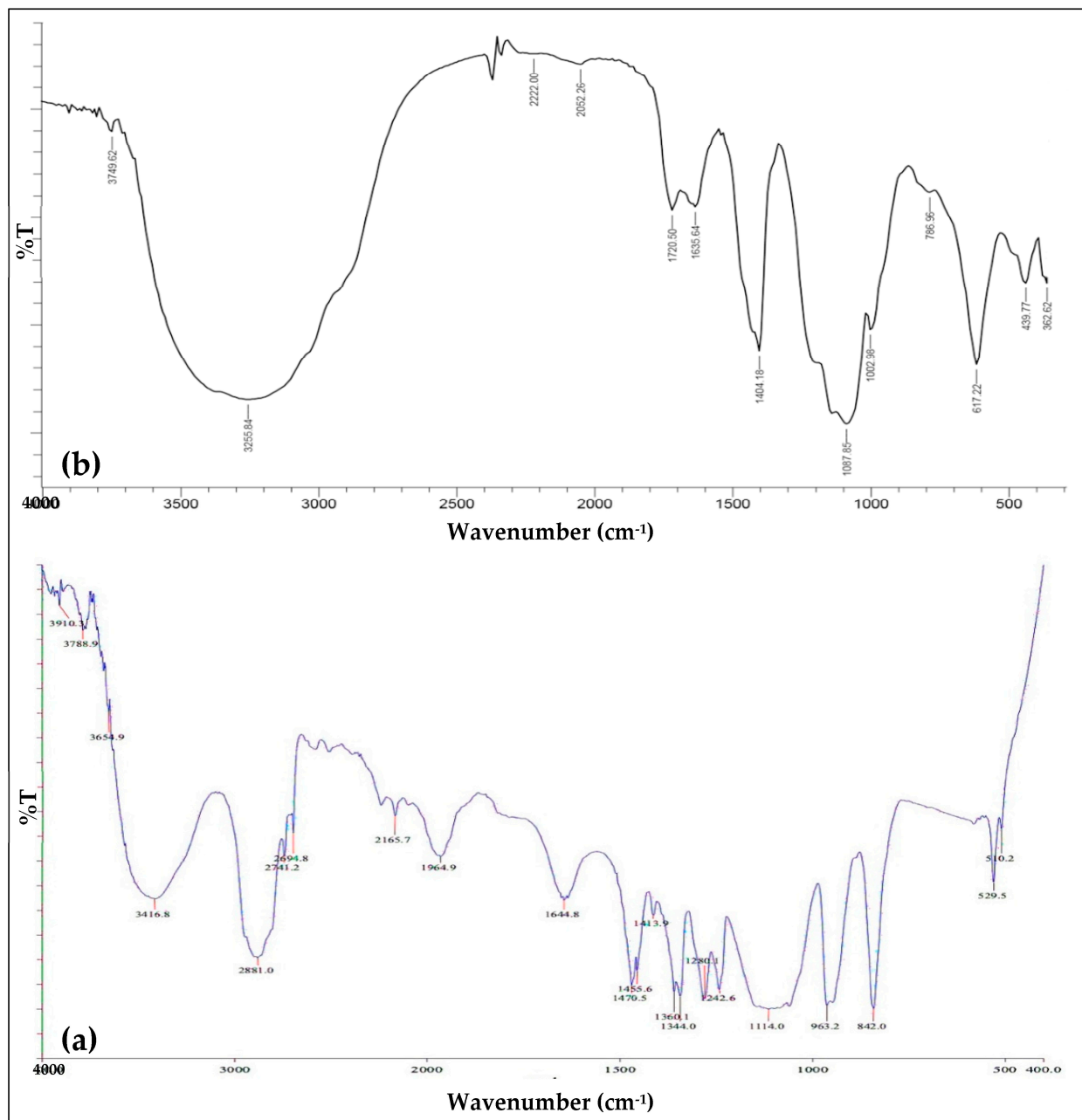


Figure 1. FT-IR spectra of PEG-6000 (a) and Zr_{0.90}Mg_{0.10}O₂ after drying at 120 °C (b) [1].

As shown by the XRD analysis in Table 2, the drying at 120 °C only resulted in a low crystallinity of ~50%. The size of the crystallites observed ranged from sub-micron to micron, with the smallest crystallite of t -ZrO₂ at 164 nm and ZrSiO₄ at 202 nm, shown in Zr_{0.95}Mg_{0.05}O₂, while the largest crystallite was observed in Zr_{0.99}Mg_{0.01}O₂, at 771 nm and 4003 nm for t -ZrO₂ and ZrSiO₄, respectively. This is in line with previous findings that nanoparticle Mg-PSZ was only observed after calcination at a temperature of 600–1000 °C [1]. Magnesium oxide as a stabilizing agent in the preparation of zirconia nano-powders has been demonstrated to have an inhibitory effect on the growth of

particle grains and lead to smaller size and more uniform distribution compared with non-stabilized zirconia [33,34].

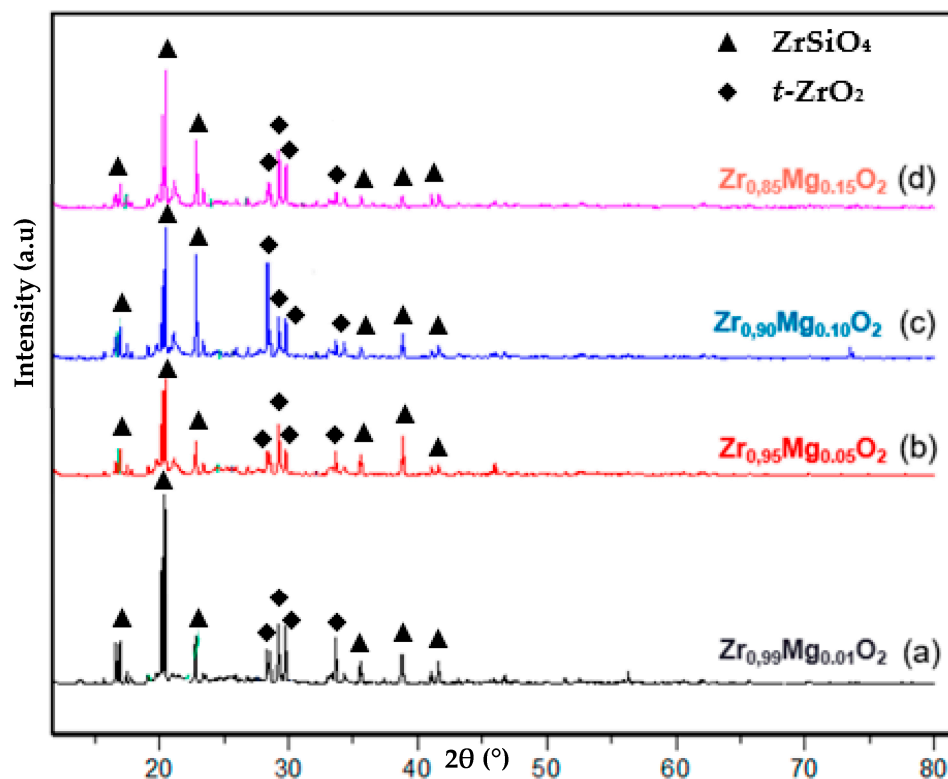


Figure 2. Diffractogram of Mg-PSZ drying 120 °C $Zr_{0.99}Mg_{0.01}O_2$ (a), $Zr_{0.95}Mg_{0.05}O_2$ (b), $Zr_{0.90}Mg_{0.10}O_2$ (c), and $Zr_{0.85}Mg_{0.15}O_2$ (d).

Table 2. Crystallinity and crystallite size of Mg-PSZ dried at 120 °C.

Samples	Crystallinity (%)	Crystal Size $ZrSiO_4$ (nm)	Crystal Size $t-ZrO_2$ (nm)
$Zr_{0.99}Mg_{0.01}O_2$	53.56	4002	771
$Zr_{0.95}Mg_{0.05}O_2$	51.70	202	164
$Zr_{0.90}Mg_{0.10}O_2$	52.41	425	193
$Zr_{0.85}Mg_{0.15}O_2$	50.87	2434	225

Next, we observed a structural transformation in ZrO_2 after calcination, as shown by the XRD analysis in Figure 3. After being calcined at 800 °C, only $t-ZrO_2$ were observed in all the specimens, as shown in Figure 3. Peaks in all of the Mg-PSZ showed identical principal peaks at 2θ of 30.40°, 34.49°, 35.40°, 50.25°, 50.74°, 59.36°, 60.20°, 62.86, and 74.63°, corresponding to the crystal planes (101), (002), (110), (112), (200), (103), (211), (202), and (220). Those peaks and crystal planes are all associated with $t-ZrO_2$ (JCPDS PDF2 no. 791770). This is in accordance with a previous study that reported that MgO doping in ZrO_2 resulted in a $t-ZrO_2$ structure after calcination at 800 °C [1]. In a former study of Mg-PSZ, a minimum 16% of MgO was required to stabilize ZrO_2 and form $t-ZrO_2$, [35]. In another study, MgO at 10% was shown to be sufficient as a stabilizer in obtaining a tetragonal phase [36]. However, we observed that a smaller concentration of MgO at 1% and 5% may also lead to stabilized $t-ZrO_2$.

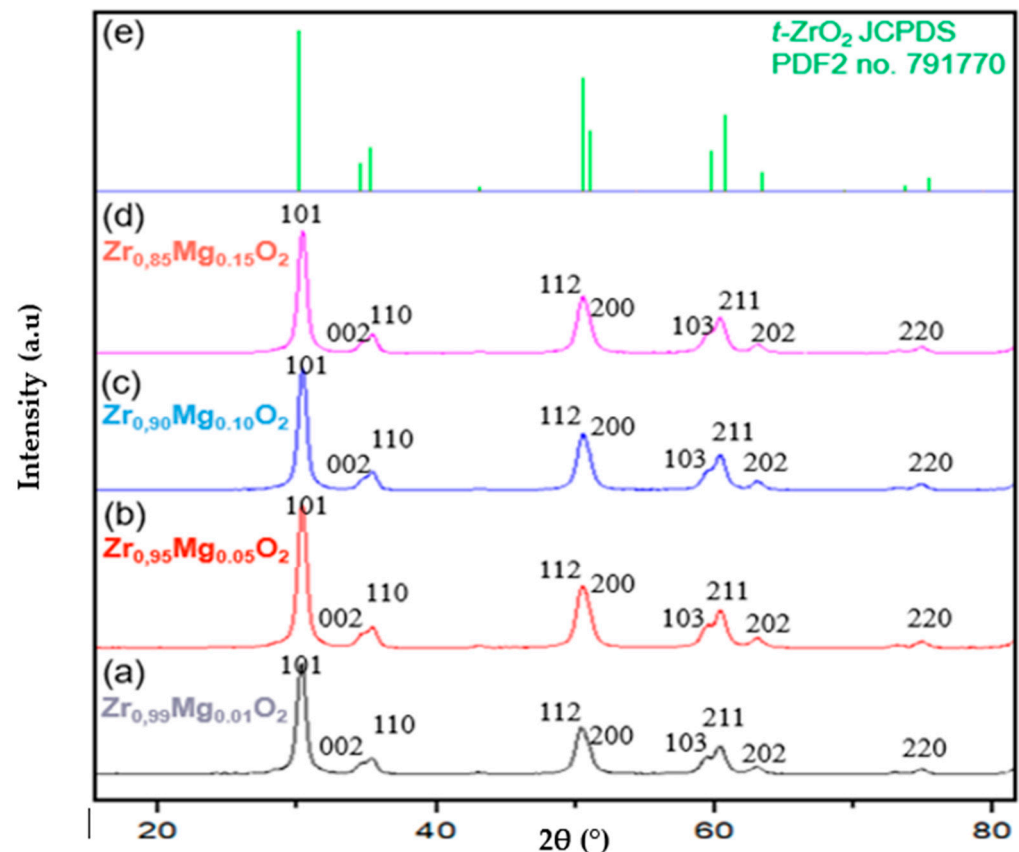
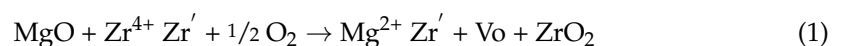


Figure 3. Diffractogram of $Zr_{0.99}Mg_{0.01}O_2$ (a), $Zr_{0.95}Mg_{0.05}O_2$ (b), $Zr_{0.90}Mg_{0.10}O_2$ (c), $Zr_{0.85}Mg_{0.15}O_2$ (d), and $t\text{-ZrO}_2$ JCPDS PDF2 no. 791770 (e).

The stabilization of the ZrO_2 structure is caused by cations having a larger radius than Zr^{4+} replacing some of the Zr^{4+} lattice point positions in the ZrO_2 lattice with doping oxides to become pure ZrO_2 material [37]. Meanwhile, a substituted solid solution is formed in this ZrO_2 material through doping, which maintains the stable phase structure of the doped ZrO_2 material at room temperature, thereby achieving a toughening effect for pure ZrO_2 materials and leading to the formation of partially stabilized zirconia materials (PSZ) [38,39]. The mechanism of MgO in stabilizing ZrO_2 can be explained by the difference in charge between the Zr^{4+} ion and the Mg^{2+} . The stabilization is caused by a defect in the lattice of a crystal due to doping ions having a lower valence, which leads to oxygen vacancy, as explained in the following equation.



The reduction of oxygen takes place to balance the positive charge, leading to a neutrally charged Mg-doped ZrO_2 without free electrons [40]. Oxygen vacancies in the zirconia lattice can reduce the transformation temperature of the transition or metastable phase, and stabilize and increase the concentration of the tetragonal phase in the Zr- ZrO_2 binary system region [12]. The amount of oxygen vacancies in the ZrO_2 lattice influences the formation of a different phase of ZrO_2 , where the tetragonal phase is formed with a low oxygen vacancy, while the cubic phase is formed with a higher oxygen vacancy [18,41].

As shown by the XRD analysis in Table 3, all the specimens of Mg-PSZ calcined at 800 °C have a high crystallinity, with the highest crystallinity of 96.35% being shown in $Zr_{0.90}Mg_{0.10}O_2$ and the lowest at 91.28% shown in $Zr_{0.99}Mg_{0.01}O_2$. The size of the crystallite in all the samples were found to be in a nanometer scale. However, there was an increase in size along with an increase in Mg content, which was likely contributed by Mg.

Table 3. Crystallinity and crystallite size of calcined Mg-PSZ 800 °C.

Sample	Crystallinity (%)	Crystal Size <i>t</i> -ZrO ₂ (nm)
Zr _{0.99} Mg _{0.01} O ₂	91.28	78
Zr _{0.95} Mg _{0.05} O ₂	95.32	81
Zr _{0.90} Mg _{0.10} O ₂	96.35	97
Zr _{0.85} Mg _{0.15} O ₂	95.85	112

The overall obtained crystal is *t*-ZrO₂, as shown in Table 4. The sample Zr_{0.95}Mg_{0.05}O₂ has the largest tetragonal phase composition of 99.5%, with a monoclinic phase composition of 0.5% as impurities, while the variation with the lowest tetragonal phase composition is Zr_{0.85}Mg_{0.15}O₂ at 96.2% and the monoclinic phase as an impurity is 2.7%. When compared with dental implants with ceramic material yttria-stabilized tetragonal zirconia (Y-TZP) based on ISO 13356:2015 Third Edition, the synthesized partially stabilized magnesia zirconia (Mg-PSZ) meets one of the requirements, which is that the minimum composition of the monoclinic phase is below 20%. Mass fraction has been successfully obtained with very low monoclinic fraction compositions ranging from 0.5 to 2.7% for all synthesized Mg-PSZ.

Table 4. Mg-PSZ phase percentage.

Samples Mg-PSZ	Monoclinic (%)	Tetragonal (%)
Zr _{0.99} Mg _{0.01} O ₂	2.1	97.9
Zr _{0.95} Mg _{0.05} O ₂	0.5	99.5
Zr _{0.90} Mg _{0.10} O ₂	2.4	97.6
Zr _{0.85} Mg _{0.15} O ₂	2.7	96.2

2.2. Mechanical Properties of Mg-PSZ

Hardness is one of the most important parameters for comparing dental implant material properties, as it is used to find the suitability of the clinical use of biomaterials [42]. A study explained that the addition of 10% MgO concentration increased the hardness of Vickers ZrO₂ from 554 to 6350 MPa [20]. The increased mechanical properties in *t*-ZrO₂ was due to the presence of MgO, which prevents the reverse allotropic transformation of zirconia. In general, an increase in hardness that requires a decrease in porosity is known as the Duckworth–Knudsen model [43]. The results of the hardness test are shown in Table 5.

Table 5. Vickers hardness of ZrO₂ and Mg-PSZ.

Samples	Hardness (HV)	Hardness (MPa)
ZrO ₂ [21]	59.5	554
Zr _{0.99} Mg _{0.01} O ₂	407	3991
Zr _{0.95} Mg _{0.05} O ₂	98.9	969.9
Zr _{0.90} Mg _{0.10} O ₂	537	5266
Zr _{0.85} Mg _{0.15} O ₂	125	1226

The Vickers hardness test showed that doping MgO in ZrO₂ successfully increased the hardness of the ZrO₂, as shown in Table 5. Zr_{0.90}Mg_{0.10}O₂ has shown the highest Vickers hardness with a value of 5266 MPa. This obtained result is almost in accordance with a previous study that reported an increase in hardness to 6350 MPa after an addition of 10% MgO in ZrO₂ [20]. However, we did not observe a consistent trend in the increase in hardness. This is most likely due to the different surface roughness of each specimen [44]. As shown in Figure 4, the Zr_{0.95}Mg_{0.05}O₂ sample showed a less flat surface, while in contrast, Zr_{0.90}Mg_{0.10}O₂ showed a flat surface. This led to different pressures in the indenter when the test was carried out. When a rough surface is stressed, the resulting pressure triangle will produce a very large distance, which will cause the calculation of the Vickers hardness value to be small. Meanwhile, lower roughness leads to a smaller triangle size and the Vickers hardness value being large.

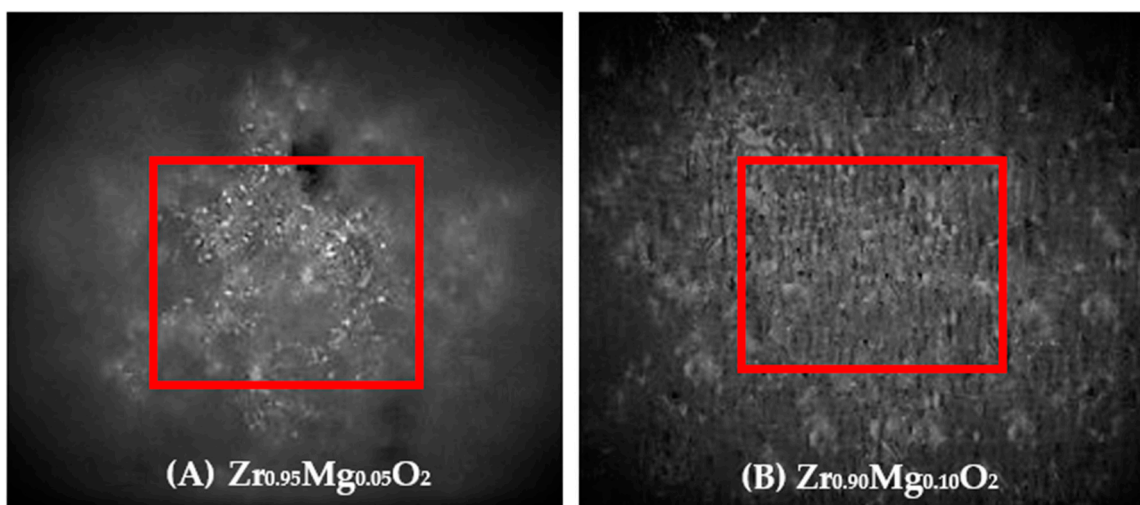


Figure 4. Magnification of 100× microvickers, Zr_{0.95}Mg_{0.05}O₂ (A) and Zr_{0.90}Mg_{0.10}O₂ (B).

2.3. Stability of Mg-PSZ

The stability test of Mg-PSZ was carried out by a simple in vitro biodegradation test. Each specimen was immersed in SBF (Simulated Body Fluid) solution for 3 days. As shown in Figure 5, the pH of the SBF solution was changed after the ZrO₂ and Mg-PSZ samples were soaked for 3 days at 37 °C.

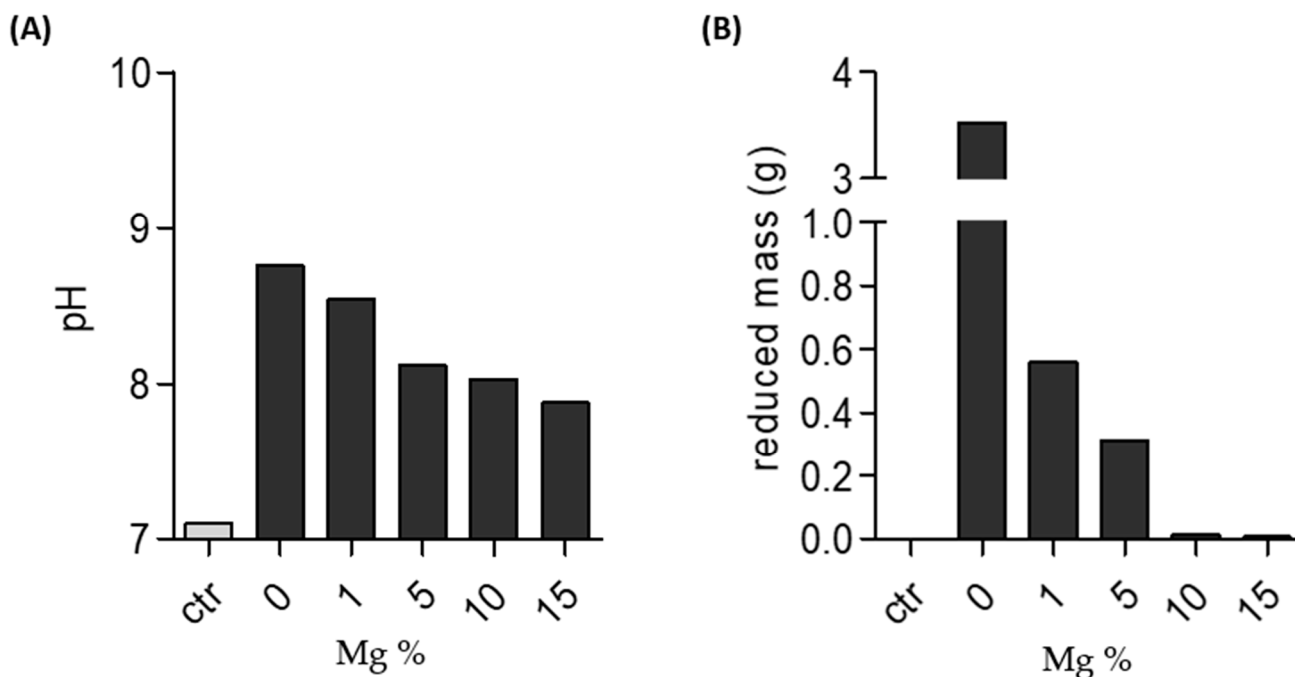
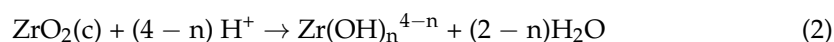


Figure 5. Stability of Zirconia and Mg-PSZ. (A) pH of solution after zirconia or Mg-PSZ soaked for 3 days in SBF. (B) Loss of weight after zirconia or Mg-PSZ soaked for 3 days in SBF. SBF solution without zirconia or Mg-PSZ was used as control.

In general, the dissolution reaction of ZrO₂ in an aqueous medium follows the equation [45]:



Soaking the sample for 3 days in SBF solution at 37 °C showed a change in pH, as shown in Figure 5A. After soaking for 3 days, a significant change in pH was found in the ZrO₂, which was at 8.76, and gradually lower changes in pH were observed in samples

with increasing MgO. Additionally, this changes in pH corresponded with mass loss, as shown in Figure 5B. Thus, the changes in pH of the SBF solution in the sample is due to the release of Zr^{4+} ions from the ZrO_2 .

The immersion of the ZrO_2 and the variation of the Mg-PSZ carried out for 3 days at 37 °C showed the largest mass change for the ZrO_2 without MgO doping with a mass loss of 3.2545 g. Testing the variation of the Mg-PSZ sample in Figure 5B shows that the degradation of the sample that occurred is strongly influenced by the concentration of the MgO used. Sample variation 4, with the addition of 15% of MgO, showed the best resistance of the material to SBF with a lost weight of 0.0069 g. These data show a correlation between changes in SBF pH and the amount of ZrO_2 sample dissolved in the SBF solution.

Based on the variation of MgO concentrations, we concluded that the greater the concentration of MgO in doping the ZrO_2 , the greater the degradation resistance of the SBF solution. However, another thing to note is that although the addition of MgO showed a significant effect on ZrO_2 resistance, further tests (in vivo tests) were needed to determine the time of osteoblast formation in the bone and the effect of pH on osteoblast cells. This is because changes in pH in the osteoblast cell environment can provide an inflammatory response so that the formation of osteoblast cells becomes slow [46].

3. Materials and Methods

Materials used were $(NH_4)HCO_3$ (PT. Brataco, Jakarta, Indonesia), H_2SO_4 95–97% (Merck KGaA, Darmstadt, Germany), Carboxyl Methyl Cellulose (PT. Brataco, Jakarta, Indonesia), $MgSO_4 \cdot 7H_2O$ (Merck KGaA, Darmstadt, Germany), PEG-6000 (PT. Brataco, Jakarta, Indonesia), Simulated Body Fluid (SBF) (MaxLab, Jakarta, Indonesia), and zirconium oxyhydroxide ($ZrO(OH)_2$) prepared from local zirconium silicates from the province of West Kalimantan, Indonesia. First, the Mg-PSZ was synthesized from $ZrO(OH)_2$, $MgSO_4 \cdot 7H_2O$ as dopant, and PEG-6000 for template. The obtained structure of Mg-PSZ was then analyzed using XRD. Next, physical properties were analyzed by means of hardness and stability in biological environment.

3.1. Preparation of Crystals

Prior to the synthesis, zirconium oxyhydroxide was analyzed using XRF to determine the ZrO_2 content. Next, 60 g of $ZrO(OH)_2$ was dissolved in 25 mL of 17.74 M H_2SO_4 . The pH was adjusted to 3.0 by adding appropriate amount of 1 M $(NH_4)HCO_3$. Subsequently, $MgSO_4 \cdot 7H_2O$ was added in a molar ratio of 0.01, 0.05, 0.10, or 0.15 compared with Zr. Afterwards, 10% PEG-6000 in water was added to the mixture of Mg:Zr at a volume ratio of 1:15 (PEG-6000:Mg-Zr). Mixture was continuously stirred until homogeneous for 1 h, then heated at 120 °C for 3 h and rested overnight at RT. The next day, gel was filtered and followed by drying at 100 °C for 2 days to obtain dry solid material. Finally, solid material was rinsed with hot deionized water to remove impurities and then dried again at 100 °C for 1 day. After drying, powder was collected for FTIR, XRD, and further processing. Powder was then calcined at 800 °C and further characterized using XRD and TEM [1,2].

3.2. Mechanical Properties

To evaluate the hardness of Mg-PSZ, material was made into a 2 cm × 2 cm × 1 cm block for microvickers test. The load was set at 200 g.f for 10 s. Vickers hardness was then calculated using the following formula [47]:

$$HV = \frac{2P \sin\left(\frac{\alpha}{2}\right)}{d^2} \quad (3)$$

HV = Vickers Hardness, P = Load (kg.f), α = opposite angle of the indenter, and d = the average indentation diagonal.

3.3. Stability

To examine the stability in a biological setting, Mg-PSZ was soaked in a simulated body fluid, followed by measurement of pH in the solution and changes in specimen weight, according to previous study [48]. Briefly, prepared Mg-PSZ block was soaked in a simulated body fluid which has very similar ionic composition to human blood plasma. The ion contents are shown in Table 6. After soaked for 3 days at 37 °C, each Mg-PSZ was weighted to measure changes compared with initial weight before soaking. Furthermore, pH of SBF before and after the experiment was measured.

Table 6. Comparison of ions in SBF and blood plasma in the body [49].

	Ion Concentration (mM)						
	Na ⁺	K ⁺	Mg ²⁺	Ca ²⁺	Cl ⁻	HCO ₃ ⁻	HPO ₄ ⁻
Plasma	142.0	5.0	1.5	2.5	103.0	27.0	1.0
SBF	142.0	5.0	1.5	2.5	148.8	4.2	1.0

4. Conclusions

The introduction of MgO led to the creation of *t*-ZrO₂. A heating process at 800 °C enhanced the structural crystallinity and further stabilized ZrO₂. While the utmost *t*-ZrO₂ composition (99.5%) was attained with 5% MgO (Zr_{0.95}Mg_{0.05}O₂), the ZrO₂ sample containing 10% MgO (Zr_{0.95}Mg_{0.05}O₂) exhibited the highest level of crystalline quality at 96.35%. Moreover, ZrO₂ containing 10% MgO exhibited the highest Vickers hardness at 5266 MPa. Conversely, elevated concentrations of MgO resulted in larger crystal sizes and improved resistance in biological environments.

Author Contributions: Conceptualization, D.Y., E.M. and A.R.N.; methodology, D.Y., E.M. and A.R.N.; investigation, D.Y.; resources, D.Y., E.M. and A.R.N.; writing—review and editing, D.Y., E.M., D.F.M. and A.R.N.; visualization, D.Y., E.M., D.F.M. and A.R.N. All authors have read and agreed to the published version of the manuscript.

Funding: This research was funded by the Development of Technology and Industrial Policy 2020 DIPA from the Center for Ceramics, Ministry of Industry, Republic of Indonesia. This work was also supported by Universitas Padjadjaran through the Hibah Academic Leadership Grant (ALG) schema 1549/UN6.3.1/PT.00.2023. by providing financial support for this research.

Institutional Review Board Statement: Not applicable.

Informed Consent Statement: Not applicable.

Data Availability Statement: Not applicable.

Conflicts of Interest: The authors declare no conflict of interest.

Sample Availability: Not applicable.

References

1. Wahyudi, K.; Maryani, E.; Arifiadi, F.; Rostika, A.; Yusuf, D.; Manullang, R.J.; Suyanti; Septawendar, R. Low-Calcination Temperatures of Magnesia Partially Stabilized Zirconia (Mg-PSZ) Nanoparticles Derived from Local Zirconium Silicates. *Mater. Res. Express* **2021**, *8*, 045022. [CrossRef]
2. Yusuf, D.; Septawendar, R.; Noviyanti, A.R. Effect of Sintering on Phase Transformation Behavior and Morphology of Calcinated 5 Wt% Mg-PSZ. *Res. J. Chem. Environ.* **2022**, *26*, 1–5. [CrossRef]
3. Baig, M.N.; Khalid, F.A.; Khan, F.N.; Rehman, K. Properties and Residual Stress Distribution of Plasma Sprayed Magnesia Stabilized Zirconia Thermal Barrier Coatings. *Ceram. Int.* **2014**, *40*, 4853–4868. [CrossRef]
4. Kobayashi, E.; Matsumoto, S.; Doi, H.; Yoneyama, T.; Hamanaka, H. Mechanical Properties of the Binary Titanium-Zirconium Alloys and Their Potential for Biomedical Materials. *J. Biomed. Mater. Res.* **1995**, *29*, 943–950. [CrossRef]
5. do Nascimento, R.O.; Chirani, N. Shape-Memory Polymers for Dental Applications. In *Shape Memory Polymers for Biomedical Applications*; Woodhead Publishing: Cambridge, UK, 2015; pp. 267–280. [CrossRef]
6. Reti, A.; Mridha, S. Silver: Alloying, Properties, and Applications. In *Reference Module in Materials Science and Materials Engineering*; Elsevier: Amsterdam, The Netherlands, 2016. [CrossRef]

7. Vaidya, A.; Pathak, K. Mechanical Stability of Dental Materials. In *Applications of Nanocomposite Materials in Dentistry*; Woodhead Publishing: Cambridge, UK, 2019; pp. 285–305. [[CrossRef](#)]
8. Dunne, N.; Mitchell, C. Biomedical/Bioengineering Applications of Carbon Nanotube-Based Nanocomposites. In *Polymer–Carbon Nanotube Composites: Preparation, Properties and Applications*; Woodhead Publishing: Cambridge, UK, 2011; pp. 676–717. [[CrossRef](#)]
9. Matei, M.; Voinea, E.A.; Rică, R.; Manolea, H.; Mogoantă, L.; Salan, A.; Rică, A.; Dinescu, V.C.; Cioateră, N. New Zirconia-Based Materials for Dental Applications. Structural, Morphological and Histological Evaluation. *Ceram. Int.* **2019**, *45*, 14859–14866. [[CrossRef](#)]
10. Heuer, C.; Storti, E.; Graule, T.; Aneziris, C.G. Electrospinning of Y₂O₃- and MgO-Stabilized Zirconia Nanofibers and Characterization of the Evolving Phase Composition and Morphology during Thermal Treatment. *Ceram. Int.* **2020**, *46*, 12001–12008. [[CrossRef](#)]
11. Koltsov, I.; Smalc-Koziorowska, J.; Przeźniak-Welenc, M.; Małysa, M.; Kimmel, G.; McGlynn, J.; Ganin, A.; Stelmakh, S. Mechanism of Reduced Sintering Temperature of Al₂O₃–ZrO₂ Nanocomposites Obtained by Microwave Hydrothermal Synthesis. *Materials* **2018**, *11*, 829. [[CrossRef](#)]
12. Štefanić, G.; Musić, S. Factors Influencing the Stability of Low Temperature Tetragonal ZrO₂. *Croat. Chem. Acta* **2002**, *75*, 727–767.
13. Özkurt, Z.; Kazazoğlu, E. Clinical Success of Zirconia in Dental Applications. *J. Prosthodont.* **2010**, *19*, 64–68. [[CrossRef](#)]
14. Deirmina, F.; Pellizzari, M. Mechanical Properties and Tempering Resistance of an Ultrafine Grained Tool Steel-PSZ Composite Fabricated by High Energy Mechanical Milling and Spark Plasma Sintering. *Mater. Sci. Eng. A* **2020**, *786*, 139428. [[CrossRef](#)]
15. Wijayanti, R.; Rosmayanti, I.; Wahyudi, K.; Maryani, E.; Hernawan, H.; Septawendar, R. Preparation of Magnesia Partially Stabilized Zirconia Nanomaterials from Zirconium Hydroxide and Magnesium Carbonate Precursors Using PEG as a Template. *Crystals* **2021**, *11*, 635. [[CrossRef](#)]
16. Yoon, S.; Van Tyne, C.J.; Lee, H. Effect of Alumina Addition on the Microstructure and Grain Boundary Resistance of Magnesia Partially-Stabilized Zirconia. *Curr. Appl. Phys.* **2014**, *14*, 922–927. [[CrossRef](#)]
17. Soylemez, B.; Sener, E.; Yurdakul, A.; Yurdakul, H. Fracture Toughness Enhancement of Ytria-Stabilized Tetragonal Zirconia Polycrystalline Ceramics through Magnesia-Partially Stabilized Zirconia Addition. *J. Sci. Adv. Mater. Devices* **2020**, *5*, 527–534. [[CrossRef](#)]
18. Doleker, K.M.; Ozgurluk, Y.; Ozkan, D.; Mesekiran, N.; Karaoglanli, A.C. Comparison of Microstructures and Oxidation Behaviors of Ytria and Magnesia Stabilized Zirconia Thermal Barrier Coatings (TBC). *Mater. Tehnol.* **2018**, *52*, 315–322. [[CrossRef](#)]
19. Chevalier, J.; Gremillard, L.; Virkar, A.V.; Clarke, D.R. The Tetragonal-Monoclinic Transformation in Zirconia: Lessons Learned and Future Trends. *J. Am. Ceram. Soc.* **2009**, *92*, 1901–1920. [[CrossRef](#)]
20. Savchenko, N.L.; Sablina, T.Y.; Sevostyanova, I.N. Influence of Porosity on the Structural-Phase State of ZrO₂-Y₂O₃ Ceramics. *AIP Conf. Proc.* **2019**, *2167*, 020313. [[CrossRef](#)]
21. Sallemi, I.; Bouaziz, J.; Ben Ayed, F. The Effect of Adding Magnesium Oxide on the Mechanical Properties of the Tricalcium Phosphate-Zirconia Composites. *Mater. Chem. Phys.* **2015**, *151*, 50–59. [[CrossRef](#)]
22. Azhar, A.Z.A.; Mohamad, H.; Ratnam, M.M.; Ahmad, Z.A. The Effects of MgO Addition on Microstructure, Mechanical Properties and Wear Performance of Zirconia-Toughened Alumina Cutting Inserts. *J. Alloys Compd.* **2010**, *497*, 316–320. [[CrossRef](#)]
23. Bramhe, S.N.; Lee, Y.P.; Nguyen, T.D.; Kim, T.N. Synthesis of Ytria Stabilized Zirconia by Sol-Gel Precipitation Using PEG and PVA as Stabilizing Agent. *Korean J. Mater. Res.* **2013**, *23*, 441–446. [[CrossRef](#)]
24. George, S.M.; Haycock, P.W.; Ormerod, R.M. The Mechanism of Corrosion of Aluminium Zirconium Silicate (AZS) Material in the Float Glass Furnace Regenerator. *J. Eur. Ceram. Soc.* **2018**, *38*, 2202–2209. [[CrossRef](#)]
25. Su, S.; Du, F.S.; Li, Z.C. Facile Synthesis of a Degradable Poly(ethylene glycol) Platform with Tunable Acid Sensitivity at Physiologically Relevant pH. *Macromolecules* **2018**, *51*, 6571–6579. [[CrossRef](#)]
26. Ansari, A.; Ali, A.; Asif, M.; Shamsuzzaman, S. Microwave-Assisted MgO NP Catalyzed One-Pot Multicomponent Synthesis of Polysubstituted Steroidal Pyridines. *New J. Chem.* **2018**, *42*, 184–197. [[CrossRef](#)]
27. Lin, Z.; Han, X.; Wang, T.; Li, S. Effects of Adding Nano Metal Powders on Thermo-oxidative Degradation of Poly(Ethylene Glycol). *J. Therm. Anal. Calorim.* **2008**, *91*, 709–714. [[CrossRef](#)]
28. Boughen, L.; Liggat, J.; Ellis, G. Thermal degradation of polyethylene glycol 6000 and its effect on the assay of macroprolactin. *Clin. Biochem.* **2010**, *43*, 750–753. [[CrossRef](#)]
29. Kodal, M.; Karakaya, N.; Alchekh Wis, A.; Ozkoc, G. Thermal Properties (DSC, TMA, TGA, DTA) of Rubber Nanocomposites Containing Carbon Nanofillers. In *Carbon-Based Nanofiller and Their Rubber Nanocomposites*; Yaragalla, S., Mishra, R.K., Thomas, S., Kalarikkal, N., Maria, H.J., Eds.; Elsevier: Amsterdam, The Netherlands, 2019; pp. 325–366. [[CrossRef](#)]
30. Liu, J.; Song, J.; Qi, T.; Zhang, C.; Qu, J. Controlling the Formation of Na₂ZrSiO₅ in Alkali Fusion Process for Zirconium Oxychloride Production. *Adv. Powder Technol.* **2016**, *27*, 1–8. [[CrossRef](#)]
31. National Center for Biotechnology Information. PubChem Compound Summary for CID 61775, Zirconium Silicate. Available online: <https://pubchem.ncbi.nlm.nih.gov/compound/Zirconium-silicate> (accessed on 8 August 2023).
32. Daou, E.E. The zirconia ceramic: Strengths and weaknesses. *Open Dent. J.* **2014**, *8*, 33–42. [[CrossRef](#)]
33. Zhao, L.; Yao, S.; Li, Y.Q.; Zhao, Z.L.; Xue, Q.H. Effects of Calcium Oxide and Magnesium Oxide Stabilizing Agents on the Critical Transformation Size of Tetragonal Zirconia. *Mater. Sci. Forum* **2020**, *980*, 15–24. [[CrossRef](#)]
34. Taeh, A.; Othman, F.; Abdul-Hameed, A. Effect of Adding MgO on Microstructure of Zirconia Toughened Alumina (ZTA) Composite for Medical Applications. *Eng. Technol. J.* **2022**, *40*, 1–13. [[CrossRef](#)]

35. Duwez, P.; Odell, F.; Brown, F.H. Stabilization of Zirconia with Calcia and Magnesia. *J. Am. Ceram. Soc.* **1952**, *35*, 107–113. [[CrossRef](#)]
36. Jiang, L.; Guo, S.; Bian, Y.; Zhang, M.; Ding, W. Effect of Sintering Temperature on Mechanical Properties of Magnesia Partially Stabilized Zirconia Refractory. *Ceram. Int.* **2016**, *42*, 10593–10598. [[CrossRef](#)]
37. Chen, G.; Li, Q.; Ling, Y.; Zheng, H.; Chen, J.; Jiang, Q.; Li, K.; Peng, J.; Omran, M.; Gao, L. Phase Stability and Microstructure Morphology of Microwave-Sintered Magnesia-Partially Stabilised Zirconia. *Ceram. Int.* **2021**, *47*, 4076–4082. [[CrossRef](#)]
38. Bogicevic, A.; Wolverton, C.; Crosbie, G.M.; Stechel, E.B. Defect Ordering in Aliovalently Doped Cubic Zirconia from First Principles. *Phys. Rev. B* **2001**, *64*, 014106. [[CrossRef](#)]
39. Garvie, R.C.; Nicholson, P.S. Structure and Thermomechanical Properties of Partially Stabilized Zirconia in the CaO-ZrO₂ System. In *Sintering Key Papers*; Springer: Dordrecht, The Netherlands, 1990; pp. 259–273.
40. La Kilo, A.; Umamah, T.S.; Laliyo, L.A.R. Study on the Stability of Trivalent Cations Doped Zirconia through Atomistic Modeling. *J. Kim. Sains Apl.* **2019**, *22*, 129–135. [[CrossRef](#)]
41. Fabris, S.; Paxton, A.T.; Finnis, M.W. A Stabilization Mechanism of Zirconia Based on Oxygen Vacancies Only. *Acta Mater.* **2002**, *50*, 5171–5178. [[CrossRef](#)]
42. Kokubo, T. *Bioceramics and Their Clinical Applications*, 1st ed.; Kokubo, T., Ed.; Elsevier: Amsterdam, The Netherlands, 2008; Volume 1.
43. Lopes, M.A.; Silva, R.F.; Monteiro, F.J.; Santos, J.D. Microstructural Dependence of Young's and Shear Moduli of P₂O₅ Glass Reinforced Hydroxyapatite for Biomedical Applications. *Biomaterials* **2000**, *21*, 749–754. [[CrossRef](#)]
44. Guštin, A.; Sedlaček, M.; Žužek, B.; Podgornik, B.; Kevorkijan, V. Analysis of the Surface-Preparation Effect on the Hardness-Measurement Uncertainty of Aluminium Alloys. *Mater. Tehnol.* **2020**, *54*, 845–852. [[CrossRef](#)]
45. Shikina, N.D.; Medvedkina, O.N.; Popova, E.S.; Tagirov, R.B.; Shazzo, Y.K.; Khodakovsky, I.L. Experimental Study of the ZrO₂ Solubility in Water Solutions of Perchloric Acid at 150 °C. *Vestn. Otd. Nauk. Zemle RAN* **2011**, *3*, NZ6099. [[CrossRef](#)]
46. Lee, Y.-I.; Kim, Y.-J. Effect of Different Compositions on Characteristics and Osteoblastic Activity of Microporous Biphasic Calcium Phosphate Bioceramics. *Mater. Technol.* **2017**, *32*, 496–504. [[CrossRef](#)]
47. Davari, A.; Daneshkazemi, A.; Ataei, E.; Vatanpour, M.; Abdollahi, H. Effects of Bleaching and Remineralising Agents on the Surface Hardness of Enamel. *J. Dent. Shiraz Univ. Med. Sci.* **2012**, *13*, 156–163.
48. Kaewsichan, L.; Riyapan, D.; Prommajan, P.; Kaewsrichan, J. Effects of Sintering Temperatures on Micro-Morphology, Mechanical Properties, and Bioactivity of Bone Scaffolds Containing Calcium Silicate. *ScienceAsia* **2011**, *37*, 240. [[CrossRef](#)]
49. Kokubo, T.; Takadama, H. How Useful Is SBF in Predicting in Vivo Bone Bioactivity? *Biomaterials* **2006**, *27*, 2907–2915. [[CrossRef](#)] [[PubMed](#)]

Disclaimer/Publisher's Note: The statements, opinions and data contained in all publications are solely those of the individual author(s) and contributor(s) and not of MDPI and/or the editor(s). MDPI and/or the editor(s) disclaim responsibility for any injury to people or property resulting from any ideas, methods, instructions or products referred to in the content.